

***Performance Evaluation for a 10 kW Solar Organic Rankine Cycle Power System
to Operate in the UK Climate Conditions***

Khaled Hossin, Northumbria University, UK
Khamid Mahkamov, Northumbria University, UK

The European Conference on Sustainability, Energy & the Environment 2015
Official Conference Proceedings

Abstract

A considerable amount of medium/low grade thermal energy is available in the form of Renewable sources (solar, geothermal, biomass) and waste heat in industrial processes, which can be feasibly used to reduce consumption of fossil fuels. The Organic Rankine Cycle (ORC) technology is considered as one of the prospective technologies for utilization the above energy sources for power production. Northumbria University (UK) is working on the plans to build a small hybrid solar/biomass ORC plant and this paper presents results of the performance evaluation for a 10 kW subcritical ORC power plant for which thermal energy is provided by an array of solar evacuated tube collectors (ETCs) with heat pipes. The mathematical model of such power plant was developed and Thermolib Toolbox by EUtech Scientific Engineering GmbH was used for numerical simulations. The key components of the system include solar collectors, evaporator, expander, condenser and pump. The simulations of the plant were performed to estimate the variation of its performance during a typical day in Newcastle upon Tyne. The required areas of the solar collectors, evaporator and condenser together with the mass flow rate of the working fluid were determined for the power plant to generate 10 kWe using two organic fluids.

Keywords: Solar energy, Organic Rankine cycle, UK climate conditions

iafor

The International Academic Forum

www.iafor.org

1. Introduction

The continuous increase in the world population and the rapid development in industry have recently been leading to a tremendous increase in the global energy demand. About 80% of the current global energy consumption is estimated to be from fossil fuels [1]. Also, fossil fuels have finite sources and its consumption rate is much higher than the discovery rate of new reserves. As a result, there has been a growing concern about the fossil fuels being enough to meet the future energy needs. Furthermore, the increased consumption of fossil fuels has also caused environmental problems such as ozone depletion, global warming, and air pollution [2, 3]. These environmental problems together with the growing awareness about the fossil fuels depletion have been driving force behind searches for alternative clean sources of energy to replace fossil fuels. In the recent years, there has been a gradual shift from the overdependence on fossil fuels toward the use of renewable and cleaner energy sources such as solar energy, geothermal energy and wind energy [4].

Solar energy is considered to be one of the most reliable and world largest technically feasible renewable energy source and solar thermal low temperature applications are wide-spread across Europe and throughout the world.

In contrast to conventional Rankine cycle, organic Rankine cycle (ORC) is considered as promising technology for converting low/medium temperature energy sources into useful power, especially in the field of small and medium scale power systems (few kW – 1MW) [5, 6]. Various low-grade heat sources have been reported in the literature to be applicable with the ORC, including solar energy, geothermal energy, biomass and waste heat from industrial processes. Further benefits of this technology comprise simple construction, low maintenance, favourable operating pressures, autonomous operation and high flexibility and safety [7-11]. Moreover, installation of the ORC based systems helps in the reduction of greenhouse gas emissions which would have been produced if fossil fuels were used for the same power generation [12].

Over the last decade, small-scale solar ORCs have become a mature technology and, at the same time, remain the subject for intense research. Twomey et al. [13] tested a scroll expander in a small scale ORC (<1 kW) utilizing ETCs as a heat supply source and R134a as a working fluid. Tempsti et al. [14] analysed a 50 kW combined heat and power (CHP) ORC system powered by low-temperature geothermal and solar heat sources considering three different working fluids. Hossin et al. [15] conducted a dynamic modelling of a small-scale solar ORC system (<10 kW) using R245fa to simulate and predict the whole-day system behaviour at different seasons during the year. Quoilin et al. [6] performed modelling, sizing and evaluation of a solar ORC (3 kWe) powered by single-axis parabolic troughs and integrated with single or double stage expansion machine.

This paper provides performance evaluation and feasibility assessment for a 10 kW solar organic Rankine cycle power system to operate in the UK climate conditions using two different working fluids. The optimal operation mode for each working fluid is identified. Major technical parameters including the heat exchangers' surface area, solar collector area and the expander size are calculated. The outcome of this study will be used for designing and optimization assessment of such a system which is intended to be erected at Northumbria University, UK, and powered by a hybrid solar/biomass thermal heat source.

2. The Solar ORC System Configuration

The proposed solar ORC system consists mainly of two circuits: solar heating circuit and organic fluid circuit, as shown in Fig. 1. The key components of the system include solar collectors, evaporator, expander, condenser and working fluid pump. The evaporator has three sections, namely economizer, evaporator and superheater. The condenser is divided into two sections, namely de-superheater and condenser. Water, used as a heat transfer fluid (HTF), is heated up in the solar circuit using ETCs. The pressurized working fluid from the pump is preheated, evaporated and superheated (if required) to the maximum cycle temperature by extracting heat from the hot water in the different sections of the evaporator. The working fluid vapour then flows through the expander where useful power is generated. The working fluid at the expander exit is first cooled from superheated conditions down to saturated vapour at variable temperature in the de-superheater then it is condensed to saturated liquid in the condenser using cooling water. Liquid working fluid is pumped again in the pump to repeat the cycle. Table 1 shows the operating parameters and specifications of the considered system.

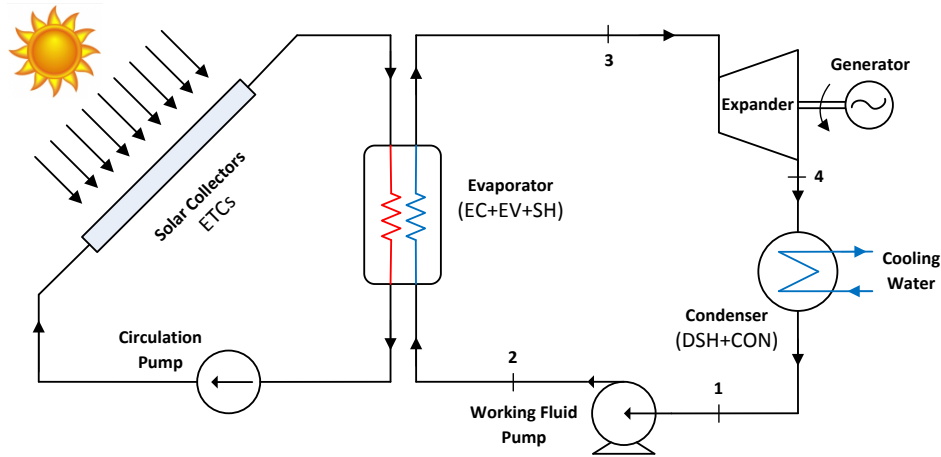


Figure 1: Schematic of the proposed solar ORC system

Table 1: Specifications of the solar ORC

| Parameter | Data |
|---------------------------------------|------|
| Gross power, kW _e | 10 |
| Heat source inlet temperature, °C | 120 |
| Cooling water inlet temperature, °C | 18 |
| Ambient temperature, °C | 25 |
| Maximum ORC operating temperature, °C | 100 |
| Maximum ORC operating pressure, bar | 30 |
| Expander isentropic efficiency, % | 70 |
| Pump isentropic efficiency, % | 80 |
| Electric generator efficiency, % | 98 |

3. Working Fluid Selection

The working fluid selection is vital for the plant performance, reliable operation and design of the key components of ORC systems [16]. Also, the working fluid selection strongly depends on the system configuration and the available heat source level [5]. In general, the correct working fluid eliminates the possibility of the turbine blades damage, caused by wet liquid droplets at the end of the expansion process [17]. Further desirable features of the working fluid include the suitable pressure range (between evaporator and condenser), high molecular weight, stability at high temperatures. Additional requirements are that these are non-toxic, non-flammable, non-corrosive, low cost and have necessary environmental safety characteristics (ODP, GWP) [18-20]. Detailed studies have been conducted on selection of appropriate working fluids for ORC system by numerous researchers [21-23]. R134a and R245fa are among prospective working fluids which are used in the commercial ORC power plants [22]. These working fluids are suitable for the heat source temperature equal to 150 °C [18, 23]. R134a and R245fa characteristics match well the heat source available in this study, with temperature of namely 120 °C and satisfy the environmental and safety considerations.

4. Thermodynamic Analysis

The following general assumptions are used in the analysis of the overall system and subsystems:

- All the components and processes are considered to be at steady state;
- The heat and pressure losses in all system components and piping are neglected;
- The expander and pump are adiabatic with fixed isentropic efficiencies;
- The changes in kinetic and potential energy are not considered.

The general steady state energy balance equation, based on the first law of thermodynamics, can be written as follows:

$$\dot{Q} - \dot{W} + \sum \dot{m}_{in} \dot{h}_{in} - \sum \dot{m}_{out} \dot{h}_{out} = 0 \quad (1)$$

where \dot{Q} and \dot{W} represent the heat transfer and work energy crossing the component boundaries and \dot{m} and \dot{h} represent the mass flow rate and the specific enthalpy of the streams of the system working fluid.

In order to develop the mathematical model for the whole system, a control volume for each component is considered. The energy balance equation (1) is then applied for each control volume.

4.1 The Solar Collector Model

The heat received by the solar collector and transferred to the HTF can be calculated based on the collector energy balance equation as a function of the collector efficiency:

$$\dot{Q}_{in} = G_t \cdot A_{col} \cdot \eta_{col} = \dot{m}_{htf} C_{p,htf} (T_{col,e} - T_{col,i}) \quad (2)$$

where G_t is the total solar irradiance on the solar collector surface, A_{col} is the collector aperture area, η_{col} is the solar collector efficiency and \dot{m}_{htf} is the hot water mass flow rate in solar heating circuit.

Newcastle upon Tyne city, located in the north east of the UK (54° 59' N latitude, 1° 37' W longitude), was selected as a location to evaluate the solar system performance. Craggs et al. [24] measured the global irradiance of Newcastle upon Tyne on vertical and horizontal surfaces for two summers (1994, 1995) and two winters (1993, 1994). They reported that the maximum measured global irradiance for the two summers were in the range of 636-703 W/m² and 913-978 W/m² for vertical and horizontal surfaces, respectively. In the winter these values decrease to 768-787 W/m² and 207-267 W/m², respectively. In this study, a value of 700 W/m² is used in the simulation. The thermal efficiency of the solar collector can be expressed in terms of the solar irradiance, mean collector temperature and ambient temperature as:

$$\eta_{col} = \alpha_0 - \alpha_1 \frac{(T_{col,m} - T_{amb})}{G_t} - \alpha_2 \frac{(T_{col,m} - T_{amb})^2}{G_t} \quad (3)$$

Here α_0 , α_1 and α_2 are efficiency equation constants for the solar collector. Table 2 presents the efficiency equation constants of the ETC for which calculations of the system performance have been carried out [14].

Table 2: ETC efficiency constants

| Constant | α_0 [-] | α_1 [W/m ² K] | α_2 [W/m ² K ²] |
|----------|----------------|------------------------------------|--|
| Value | 0.825 | 0.91 | 0.6×10^{-3} |

4.2 The Pump Model

The power consumed by the working fluid pump (see Fig.1) is calculated as:

$$\dot{W}_p = \frac{\dot{m}_{w,f} v_1 (P_2 - P_1)}{\eta_p} = \dot{m}_{w,f} (h_2 - h_1) \quad (4)$$

where $\dot{m}_{w,f}$ is the working fluid mass flow rate, η_p is the pump efficiency and P_1 , P_2 , h_1 and h_2 are the pressures and specific enthalpies of the working fluid at the pump inlet and outlet, respectively.

4.3 The Evaporator Model

The total heat transfer rate in the evaporator, \dot{Q}_e , from the HTF into the working fluid is given by:

$$\dot{Q}_e = \dot{m}_{w,f}(h_3 - h_2) = \dot{m}_{htf}C_{p,htf}(T_{e,i} - T_{e,o}) \quad (5)$$

where h_2 and h_3 are the specific enthalpies of the working fluid at the inlet and outlet of the evaporator, respectively, and $T_{e,i}$ and $T_{e,o}$ are the temperatures at the inlet and outlet of hot water stream, respectively.

4.4 The Expander Model

The working fluid vapour passes through the expander to generate the mechanical power. The expander output power is given by:

$$\dot{W}_e = \dot{m}_{w,f}(h_3 - h_{4s})\eta_i\eta_g = \dot{m}_{w,f}(h_3 - h_4)\eta_g \quad (6)$$

where η_i and η_g are the expander isentropic efficiency and the generator efficiency, respectively, h_{4s} and h_4 are the specific enthalpies of the working fluid at the expander outlet under ideal and actual conditions, respectively, and h_3 is the working fluid specific enthalpy at the expander inlet.

4.5 The Condenser Model

The exhaust vapour at the expander exit is directed to the condenser where it is converted to the liquid state by rejecting its heat to the cooling water.

The condenser heat rejection rate, \dot{Q}_c , can be expressed as:

$$\dot{Q}_c = \dot{m}_{w,f}(h_4 - h_1) = \dot{m}_w C_{p,w}(T_{c,o} - T_{c,i}) \quad (7)$$

where \dot{m}_w is the cooling water mass flow rate, and $T_{c,i}$ and $T_{c,o}$ are the cooling water temperatures at the inlet and outlet of the condenser, respectively.

4.6 Net Power Output and System Efficiencies

The net output power generated by the solar ORC system is defined as:

$$\dot{W}_{net} = \dot{W}_e - \dot{W}_p \quad (8)$$

The thermal efficiency of the ORC is the ratio of the net power output to the heat input in the evaporator. It can be expressed as:

$$\eta_{ORC} = \frac{\dot{W}_{net}}{\dot{Q}_e} \quad (9)$$

The overall efficiency of the solar ORC system can be defined as follows:

$$\eta_{sys} = \frac{\dot{W}_{net}}{G_t \cdot A_{col}} \quad (10)$$

In addition to the system efficiency, which is used to evaluate the system from a thermodynamic point of view, other parameters are needed to be defined to provide more insight into the technical feasibility and economic competitiveness of the solar ORC. These parameters include the total heat transfer surface area of the heat exchangers of the system and the volume flow ratio (VFR) between the outlet and inlet of the expander.

4.7 Calculation of the Heat Exchangers' Area

Based on the variation of heat transfer coefficient caused by different phase state, the evaporator is divided into three sections, namely, economizer (EC), evaporator (EV) and superheater (SH), while the condenser is divided into two sections, namely, de-superheater (DSH) and condenser (CON).

The logarithmic mean temperature difference (LMTD) method is used in the analysis of the heat exchangers and for the calculation of the heat transfer area [25]. The heat transfer rate in each section of the heat exchanger, \dot{Q}_i , is described as:

$$\dot{Q}_i = U_i A_i LMTD_i \quad (11)$$

where U_i and A_i are the overall heat transfer coefficient and the heat transfer area of each section, respectively. The values of the overall heat transfer coefficient for each section of the evaporator and condenser are listed in Table 3 [14]. The logarithmic mean temperature difference, $LMTD_i$, is defined as follows:

$$LMTD_i = \frac{\Delta T_{max,i} - \Delta T_{min,i}}{\ln \frac{\Delta T_{max,i}}{\Delta T_{min,i}}} \quad (12)$$

where $\Delta T_{max,i}$ and $\Delta T_{min,i}$ are the maximal and minimal temperature differences at each section terminals of the heat exchangers, respectively. The pinch point temperature differences of the evaporator and condenser used in this work are also listed in Table 3.

The total heat transfer area of the evaporator and condenser can be obtained as:

$$A_e = A_{EC} + A_{EV} + A_{SH} \quad (13)$$

$$A_c = A_{DSH} + A_{CON} \quad (14)$$

The total heat transfer surface area of the heat exchangers of the system is then given as:

$$A_{total} = A_e + A_c \quad (15)$$

Table 3: The evaporator and condenser parameters

| Evaporator | | Condenser | |
|------------------|------------------------|------------------|------------------------|
| Parameter | Value | Parameter | Value |
| U_{EC} | 250 W/m ² K | U_{OSH} | 125 W/m ² K |
| U_{EF} | 200 W/m ² K | U_{COW} | 225 W/m ² K |
| U_{SH} | 125 W/m ² K | | |
| ΔT_{ppe} | 8 K | ΔT_{ppe} | 5 K |

4.8 The Volume Flow Ratio

The volume flow ratio (VFR) is defined as the ratio between the volume flow rates at the outlet and inlet of the expander. Increased VFR values are associated with large expander size and technical complexity [26].

$$VFR = \frac{\dot{V}_1}{\dot{V}_3} \quad (16)$$

The simulation of the proposed solar ORC system was developed using Thermolib 5.2 toolbox [27], by EUtech Scientific Engineering GmbH, in a MATLAB/Simulink environment. The working fluid properties were evaluated using the built-in thermophysical properties database of Thermolib based on the real gas behaviour of Pen-Robinson Equation of State. The developed Thermolib model for the solar ORC system is illustrated in Fig 2.

5. Results and Discussions

A complete thermodynamic analysis was performed for the system shown in Fig. 1. The mass and energy balance equations are applied for each of the system components at steady state operation. The mass flow rates of the organic fluid, the corresponding HTF and cooling water were calculated. An analysis is conducted to investigate the effect of different operating parameters on the system performance (i.e. net power output, ORC efficiency and system efficiency). This parametric analysis results in achieving the optimal system performance for each working fluid. The ETC area of 180 m² was used for both cases of the working fluid in the parametric analysis.

5.1 Effect of Evaporation Pressure

The variations of system performance with the evaporation pressure for the two working fluids are shown in Figs. 3 and 4. The condensation temperature is fixed at 30 °C. As shown in Table 1, the maximum evaporation pressure is restricted to 30 bar, while the maximum value of the operating temperature is 100 °C.

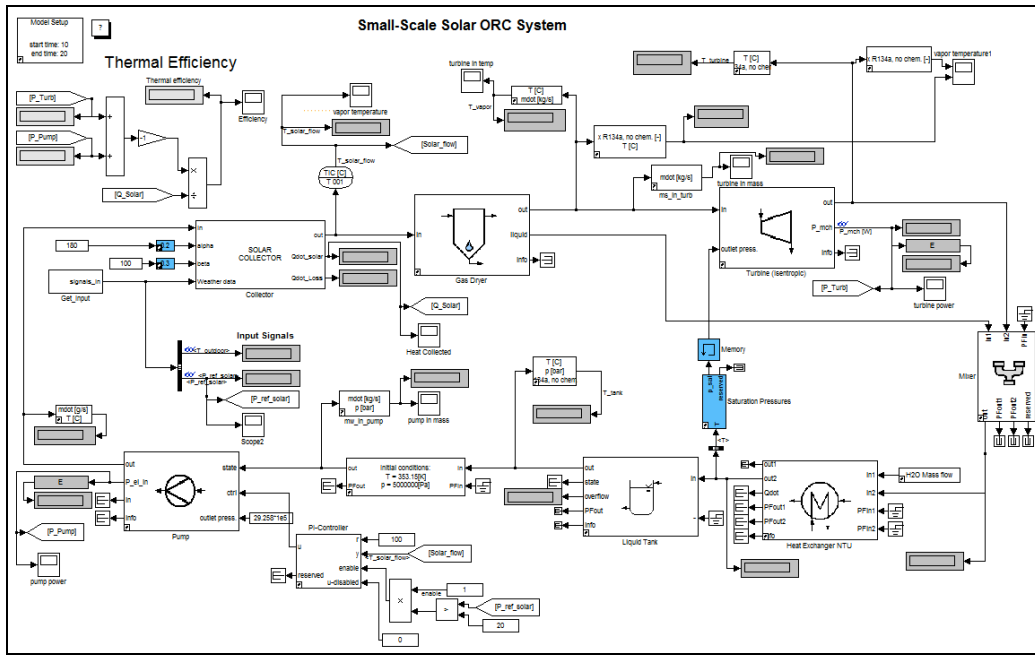


Figure 2: The developed Thermolib model for the solar ORC system

Fig. 3 shows that the net output power increases significantly with the increase of the evaporation pressure for both working fluids. The increase in the evaporation pressure yields an enthalpy increase in the expander and a decrease in the working fluid mass flow rate with domination of the former, and therefore the net output power increases. However, R245fa produces a higher net output power, compared to R134a, with lower values of evaporation pressure.

Similarly, as shown in Fig. 4, both ORC efficiency and system efficiency increase noticeably with the increase of the evaporation pressure. This is due to the significant increase of the net output power with the evaporation pressure. Also, R245fa provides higher values of ORC efficiency and system efficiency.

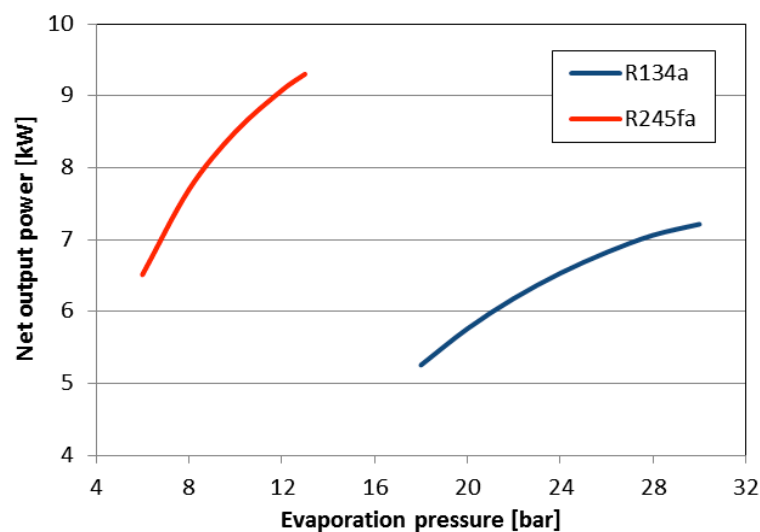


Figure 3: Variations of the net output power with evaporation pressure

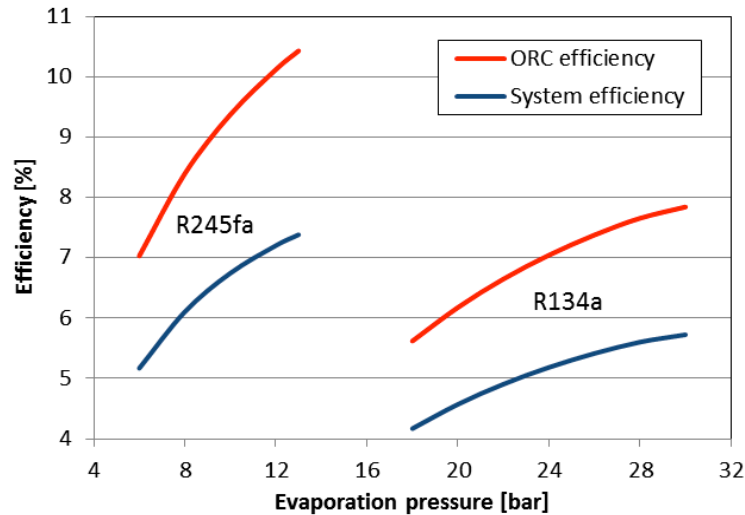


Figure 4: Variations of the ORC and system efficiency with evaporation pressure

5.2 Effect of Expander Inlet Temperature (Degree of Superheating)

Since the maximum cycle pressure is limited to 30 bar, during the superheating process, R134a should achieve the maximum cycle temperature of 100 °C. For R245fa, the maximum temperature of the cycle (100 °C) corresponds to an evaporation pressure of about 12.7 bar. The effect of degree of superheating on the system performance for R134a is illustrated in Figs. 5 and 6. The condensation temperature is set at 30 °C.

Fig. 5 presents the variation of the net output power with the degree of superheating. The net output power increases as the expander inlet temperature increases from the saturation conditions (zero superheat) towards the maximum cycle temperature of 100 °C. Fig. 6 shows a similar trend in terms of the ORC efficiency and system efficiency. These figures indicate that the net output power, ORC efficiency and system efficiency increase by about 5% with the superheating from the saturation temperature to 100 °C.

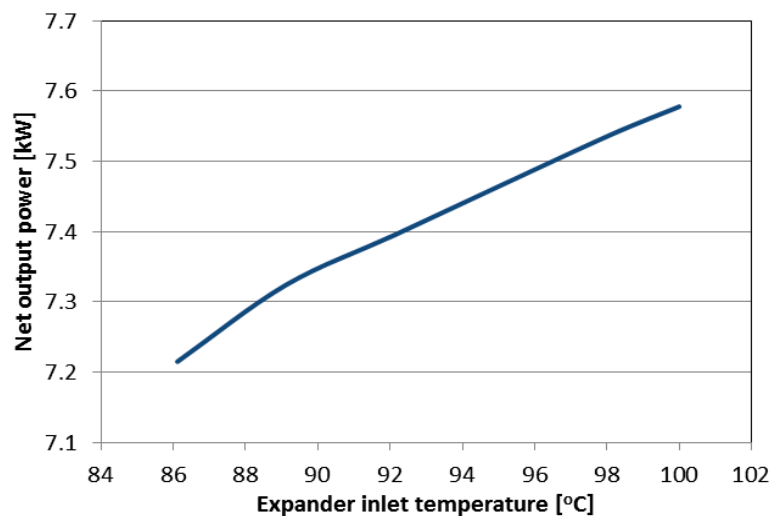


Figure 5: Variations of the net output power with expander inlet temperature (R134a)

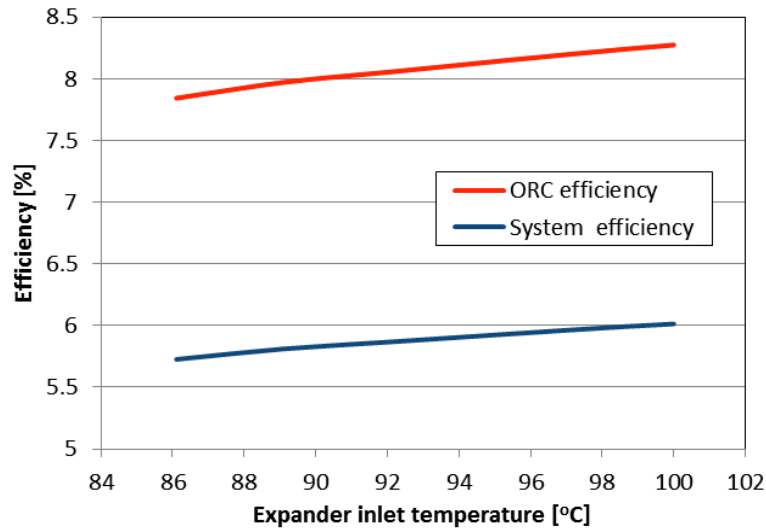


Figure 6: Variations of the ORC and system efficiency with expander inlet temperature (R134a)

5.3 The Effect of Condensation Temperature

Figs. 7 and 8 show the variations of the system performance with the condensation temperature at the optimum evaporation pressure of each working fluid. The pinch point temperature difference in the condenser is set to be 5 degrees and the condensation temperature is varied from 30 °C to 40 °C.

It can be seen in Fig. 7 that the net output power is decreasing with the rise in condensation temperature for both working fluids. R245fa produces higher values of the net output power (by about 2 kW). Fig. 8 shows that there is the same trend takes place for both the ORC efficiency and system efficiency. Decreasing the condensation temperature leads to an increase in the net output power which results in an increase in the efficiency. Also, the ORC efficiency and system efficiency are higher when R245fa is used.

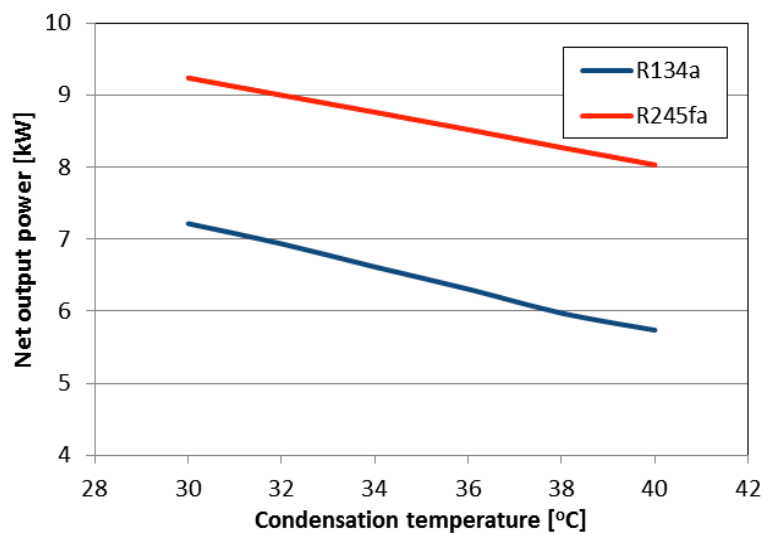


Figure 7: Variations of the net output power with condensation temperature

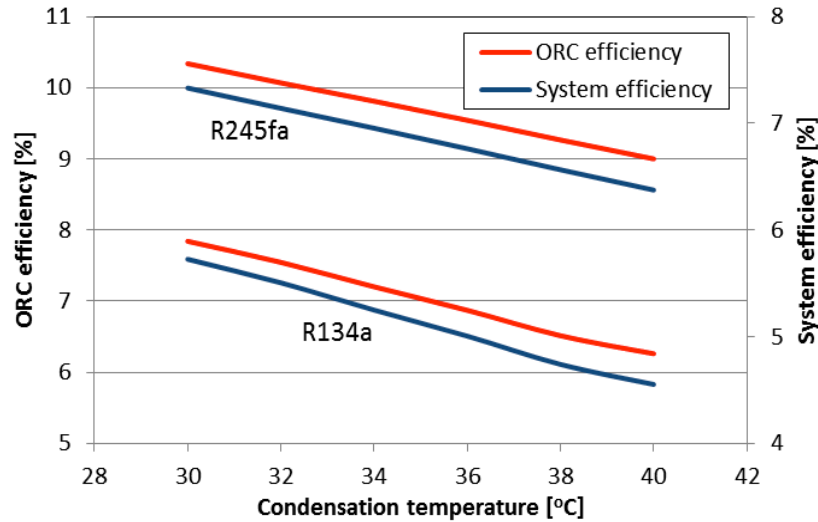


Figure 8: Variations of the ORC and system efficiency with condensation temperature

5.3 The Optimal System Performance

The optimal operating and design parameters of the 10 kW solar ORC with the heat source temperature of 120 °C are presented in Table 4 for each of the working fluids. These results were obtained at the maximum ORC operating temperature of 100 °C and condensation temperature of 30 °C. Table 4 lists thermal performance evaluation parameters and design parameters, including the total required solar collector area, total surface area of the heat exchangers and the VFR. The corresponding T-Q diagrams of the heat exchangers (evaporator and condenser) at the optimal operating conditions for R134a and R245fa are shown in Figs. 9 and 10, respectively.

It can be seen in Table 4 that the higher net output power (9.61 kW) is obtained with R245fa. This is because the system with R245fa requires less pumping power. In addition, higher ORC efficiency and system efficiency are achieved using R245fa and are equal to 10.34% and 7.33%, respectively. Also, using R245fa results in the smaller ETC area (187.2 m²) and total heat exchanger area (72.20 m²). However, application of R134a provides the lower VFR value (4.45) which indicates that a smaller expander size is needed.

Table 4: Optimal operating and design parameters

| Operating and design parameter | R134a | R245fa |
|--|-------|--------|
| Gross power, kW | 10 | 10 |
| Pump consumed power, kW | 1.22 | 0.39 |
| Net output power, kW | 8.78 | 9.61 |
| Evaporator pressure, bar | 30 | 12.72 |
| Condenser pressure, bar | 7.81 | 1.74 |
| ORC efficiency, % | 8.27 | 10.34 |
| System efficiency, % | 6.01 | 7.33 |
| Working fluid mass flow rate, kg/s | 0.523 | 0.393 |
| HTF mass flow rate, kg/s | 0.549 | 1.038 |
| Cooling water mass flow rate, kg/s | 3.093 | 2.523 |
| Expander inlet volume flow rate, m ³ /s | 0.015 | 0.044 |
| Expander volume flow ratio, - | 4.45 | 8.22 |
| Total ETC surface area, m ² | 208.6 | 187.2 |
| EC surface area, m ² | 8.95 | 5.74 |
| EV surface area, m ² | 14.94 | 20.11 |
| SH surface area, m ² | 3.67 | 0.0 |
| CON surface area, m ² | 50.30 | 41.04 |
| DSH surface area, m ² | 5.18 | 5.31 |
| Total heat exchanger area, m ² | 83.03 | 72.20 |

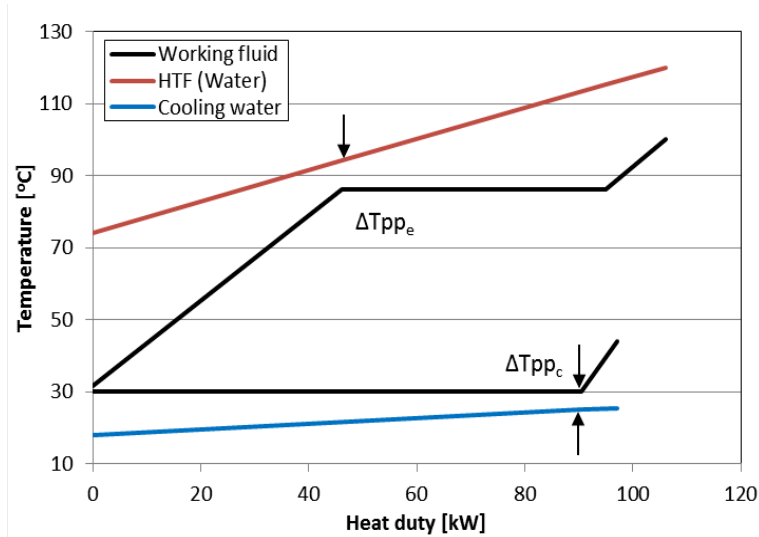


Figure 9: Evaporator and condenser T-Q diagram at optimal operating conditions (R134a)

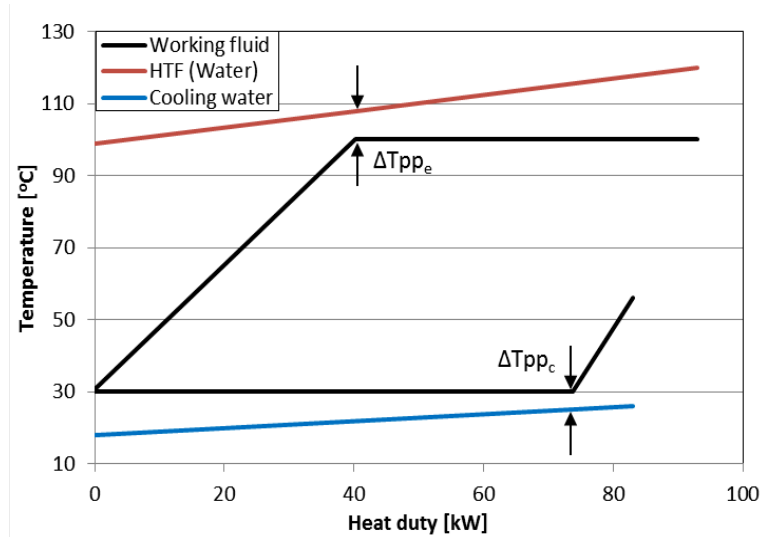


Figure 10: Evaporator and condenser T-Q diagram at optimal operating conditions (R245fa)

6. Conclusions

The performance and design parameters of the 10 kW solar ORC power system, connected to ETCs with heat pipes and to be used and operated in the UK climate conditions, were evaluated for two working fluids using thermodynamic analysis. A parametric analysis was conducted to investigate the effect of different operating conditions on the system performance in order to obtain the optimal operating and design parameters for each of the working fluids. The following are outcomes of this study:

- Both the evaporation pressure and condensation temperature have a significant influence on the system performance.
- ORC with R245fa provides higher net output power and overall system efficiency with values of 9.61 kW and 7.33%, respectively, under climatic conditions of Newcastle upon Tyne.
- ORC with R245fa requires the smaller ETC area (187.2 m²) and total heat exchanger area (72.20 m²). However, ORC with R134a has the lower VFR value (4.45), which indicates that a smaller expander size is required for the required output level.

Acknowledgment

The authors gratefully acknowledge the financial support provided by the Cultural Affairs Department of the Libyan Embassy in London.

References

- [1] EIA, *U. S. Energy Information Administration, International Energy Statistics*. Available: www.eia.gov
- [2] T. Yamamoto, T. Furuhashi, N. Arai, and K. Mori, "Design and testing of the Organic Rankine Cycle," *Energy*, vol. 26, pp. 239-251, 2001.
- [3] P. J. Mago, L. M. Chamra, K. Srinivasan, and C. Somayaji, "An examination of regenerative organic Rankine cycles using dry fluids," *Applied Thermal Engineering*, vol. 28, pp. 998-1007, 2008.
- [4] M. Aneke, B. Agnew, and C. Underwood, "Performance analysis of the Chena binary geothermal power plant," *Applied Thermal Engineering*, vol. 31, pp. 1825-1832, 2011.
- [5] A. Schuster, S. Karellas, E. Kakaras, and H. Spliethoff, "Energetic and economic investigation of Organic Rankine Cycle applications," *Applied Thermal Engineering*, vol. 29, pp. 1809-1817, 2009.
- [6] S. Quoilin, M. Orosz, H. Hemond, and V. Lemort, "Performance and design optimization of a low-cost solar organic Rankine cycle for remote power generation," *Solar Energy*, vol. 85, pp. 955-966, 2011.
- [7] S. Lecompte, S. Lemmens, H. Huisseune, M. van den Broek, and M. De Paepe, "Multi-Objective Thermo-Economic Optimization Strategy for ORCs Applied to Subcritical and Transcritical Cycles for Waste Heat Recovery," *Energies*, vol. 8, pp. 2714-2741, 2015.
- [8] D. Wei, X. Lu, Z. Lu, and J. Gu, "Performance analysis and optimization of organic Rankine cycle (ORC) for waste heat recovery," *Energy Conversion and Management*, vol. 48, pp. 1113-1119, 2007.
- [9] R. S. El-Emam and I. Dincer, "Exergy and exergoeconomic analyses and optimization of geothermal organic Rankine cycle," *Applied Thermal Engineering*, vol. 59, pp. 435-444, 9/25/ 2013.
- [10] S. Quoilin, S. Declaye, B. F. Tchanche, and V. Lemort, "Thermo-economic optimization of waste heat recovery Organic Rankine Cycles," *Applied Thermal Engineering*, vol. 31, pp. 2885-2893, 2011.
- [11] Y. Feng, Y. Zhang, B. Li, J. Yang, and Y. Shi, "Sensitivity analysis and thermoeconomic comparison of ORCs (organic Rankine cycles) for low temperature waste heat recovery," *Energy*, vol. 82, pp. 664-677, 2015.
- [12] M. Imran, B.-S. Park, H.-J. Kim, D.-H. Lee, and M. Usman, "Economic assessment of greenhouse gas reduction through low-grade waste heat recovery using organic Rankine cycle (ORC)," *Journal of Mechanical Science and Technology*, vol. 29, pp. 835-843, 2015.

- [13] B. Twomey, P. A. Jacobs, and H. Gurgenci, "Dynamic performance estimation of small-scale solar cogeneration with an organic Rankine cycle using a scroll expander," *Applied Thermal Engineering*, vol. 51, pp. 1307-1316, 2013.
- [14] D. Tempesti, G. Manfrida, and D. Fiaschi, "Thermodynamic analysis of two micro CHP systems operating with geothermal and solar energy," *Applied Energy*, vol. 97, pp. 609-617, 2012.
- [15] K. Hossin, K. Mahkamov, and B. Belgasim, "Dynamic modelling of a small-scale standalone solar organic Rankine cycle system," presented at the 4th International Conference on Nuclear and Renewable Energy Resources (NuRER2014), Antalya, Turkey, 2014.
- [16] F. Vélez, J. J. Segovia, M. C. Martín, G. Antolín, F. Chejne, and A. Quijano, "A technical, economical and market review of organic Rankine cycles for the conversion of low-grade heat for power generation," *Renewable and Sustainable Energy Reviews*, vol. 16, pp. 4175-4189, 2012.
- [17] T. Wang, Y. Zhang, Z. Peng, and G. Shu, "A review of researches on thermal exhaust heat recovery with Rankine cycle," *Renewable and Sustainable Energy Reviews*, vol. 15, pp. 2862-2871, 2011.
- [18] B. F. Tchanche, G. Lambrinos, A. Frangoudakis, and G. Papadakis, "Low-grade heat conversion into power using organic Rankine cycles – A review of various applications," *Renewable and Sustainable Energy Reviews*, vol. 15, pp. 3963-3979, 10// 2011.
- [19] A. S. Nafey and M. A. Sharaf, "Combined solar organic Rankine cycle with reverse osmosis desalination process: Energy, exergy, and cost evaluations," *Renewable Energy*, vol. 35, pp. 2571-2580, 2010.
- [20] U. Muhammad, M. Imran, D. H. Lee, and B. S. Park, "Design and experimental investigation of a 1kW organic Rankine cycle system using R245fa as working fluid for low-grade waste heat recovery from steam," *Energy Conversion and Management*, vol. 103, pp. 1089-1100, 2015.
- [21] B. Saleh, G. Koglbauer, M. Wendland, and J. Fischer, "Working fluids for low-temperature organic Rankine cycles," *Energy*, vol. 32, pp. 1210-1221, 2007.
- [22] J. Bao and L. Zhao, "A review of working fluid and expander selections for organic Rankine cycle," *Renewable and Sustainable Energy Reviews*, vol. 24, pp. 325-342, 2013.
- [23] J. Xu and C. Yu, "Critical temperature criterion for selection of working fluids for subcritical pressure Organic Rankine cycles," *Energy*, vol. 74, pp. 719-733, 2014.

- [24] C. Craggs, E. M. Conway, and N. M. Pearsall, "Statistical investigation of the optimal averaging time for solar irradiance on horizontal and vertical surfaces in the UK," *Solar Energy*, vol. 68, pp. 179-187, 2// 2000.
- [25] F. P. Incropera, D. P. Dewitt, T. L. Bergman, and A. S. Lavine, *Principles of Heat and Mass Transfer*, Seventh ed. Singapore: John Wiley & Sons, 2013.
- [26] K. Braimakis, M. Preißinger, D. Brüggemann, S. Karellas, and K. Panopoulos, "Low grade waste heat recovery with subcritical and supercritical Organic Rankine Cycle based on natural refrigerants and their binary mixtures," *Energy*, 2015.
- [27] *Thermolib*. Available: <http://www.eutech-scientific.de/products-services/thermolib.html>